Particle Dynamics and Heat Transfer under Plasma Conditions

A study was carried out of the momentum and the heat transfer to fine alumina particles injected into a DC plasma jet. Measurements are reported of particle number flux distribution, particle velocity, and in-flight particle surface temperature under different operating conditions. The results show that the particle trajectories and associated particle flux distribution depends to a large extent on the particle injection velocity. The maximum particle velocity and surface temperature are noted, however, to remain close to the centerline of the jet, independent of the particle injection conditions. The maximum surface temperature reached by the particles increases with increasing plasma power and the use of an Ar/H_2 plasma gas (17 vol. % H_2) compared to that for a pure argon plasma.

The particle velocity data are in good agreement with the predictions of a two-dimensional mathematical model used for the calculation of the particle trajectories and temperature history. The model predictions, however, agreed only in trend with the measured particle surface temperatures. Deviations between the two could still be observed at large distances from the point of injection of the powder. The computed particle number flux distributions were narrower than the measured profiles, which can be attributed to the fact that the model did not include, at this stage, turbulent particle diffusion effects.

M. Vardelle, A. Vardelle, P. Fauchais
Université de Limoges
Limoges, France

M. I. Boulos
Université de Sherbrooke
Québec, Canada

Introduction

The in-flight melting of particles under plasma conditions, whether for powder spheroidization or spray-coating, depends strongly on the proper control of the particle trajectories and their temperature history during their short residence time in the plasma stream. Our understanding of the basic phenomena involved has been aided greatly over the last few years by the availability of powerful diagnostic techniques that could be used for the measurement of the in-flight particle parameters (Boulos et al., 1986) and by the development of comprehensive theoretical models (Boulos and Fauchais, 1986).

In a previous paper (Vardelle et al., 1983) we reported a study of the plasma-particle momentum and heat transfer phenomena for single particles flowing along an axial trajectory in a DC plasma jet. Comparison of experimental measurements of particle velocity and surface temperature with the predictions of a relatively simple one-dimensional mathematical model were satisfactory as far as the particle velocity is concerned. Considerable differences were noted, however, between the measured and the computed particle surface temperatures. These were attributed to serious limitations of the experimental technique used and a number of important simplifying assumptions involved in the development of the mathematical model.

In the present study, a considerable effort has been devoted to the improvement of the experimental technique and the acquisition of new data for the particle velocity, surface temperature, and particle number flux distributions in a DC plasma jet under various operating conditions. The theoretical analysis was also improved and brought a step closer to the physical situation by developing a two-dimensional mathematical model including multiparticle injection and the Knudsen and the particle evaporation effects in the standard plasma-particle momentum and heat transfer formulation.

Experimental Techniques

A diagram of the DC plasma torch configuration used and the associated system of coordinates is given in Figure 1. The torch is of a standard design with a thoriated tungsten cathode and an

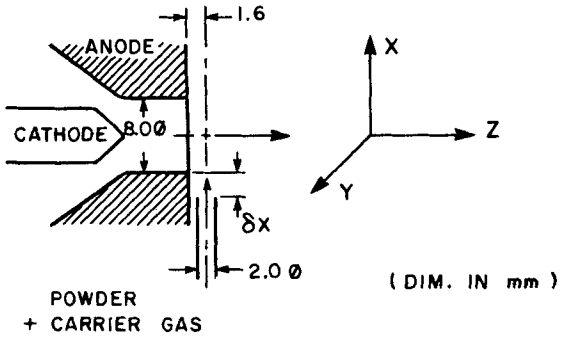

Figure 1. Plasma torch and coordinate system.

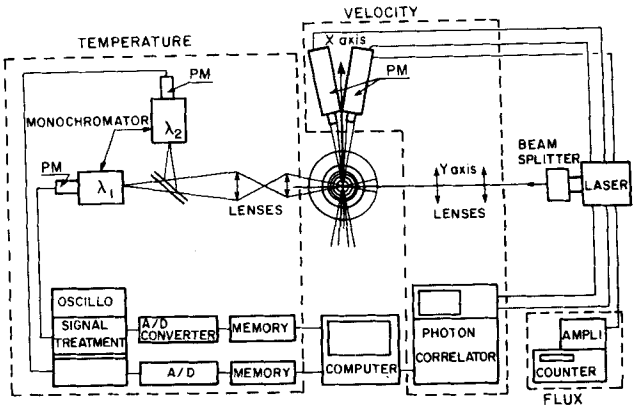

Figure 2. Experimental setup used for measurement of particle number flux, velocity, and surface temperature distributions.

8.0 mm ID water-cooled copper anode. The particles were injected inside or outside the anode nozzle at a distance of 1.6 mm upstream or downstream of the point of discharge of the plasma jet. A summary of the torch operating conditions is given in Table 1. The following measurements were carried out.

Plasma Temperature Field. This measurement was obtained by emission spectroscopy using the atomic argon lines for temperatures above 6,000 K, and thermocouples and melting point probes below that temperature. Details of the experimental technique have been described by Vardelle et al. (1980, 1983).

It should be pointed out that while the measurements were carried out with the plasma jet discharged in an ambient air atmosphere, no specific correction was made for the entrainment of the air by the jet modifying its local composition. This would have essentially no effect on the reported data up to a distance of 20 mm from the nozzle exit because of the poor mixing in this region. Beyond this point, however, the temperatures obtained from the argon lines would tend to be overestimated by about 10% in the worst case. The precision of probe measurements carried out in the plume of the plasma jet, on the other hand, is not affected by ambient air mixing.

Plasma and Particle Velocity Fields. These measurements were obtained using a time-of-flight (or two-point measurement) laser anemometer with a 1.2 W argon ion laser (λ = 514.5 nm). As shown in Figure 2, observation of the scattered light from the particles was carried out off-axis by two photomultipliers directed respectively at angles of 81° and 99° to the optical axis of the laser beam. The response time of each of the photomultipliers was 3 ns. Based on geometrical considerations, the measuring volume was estimated to be in the form of a parallelepiped of dimensions 0.1 × 0.4 × 0.5 mm in the X, Y, and Z directions, respectively.

In order to block the background plasma radiation from reaching the photomultipliers, monochromators with a band pass width of 2 Å, centered on the laser wavelength, were placed in front of each of the photomultipliers. These helped to improve considerably the performance of the laser anemometer, and allowed the observation of the scattered light from alumina particles as small as 2 μm dia. in the presence of the intense background plasma radiation. The output signal of the two photomultipliers are cross-correlated by a photon correlator (Malvern). The uncertainty associated with the reported velocity measurements is estimated to be of the order of 5–7%.

Particle Flux Number Density Distribution. This measurement was determined by counting the total pulse rate obtained from one of the photomultipliers used in the laser anemometer setup, Figure 2. The measuring volume was therefore identical to that given earlier for the anemometer. The results, however, represent the number of particles per unit time crossing a surface of dimensions 0.1 × 0.4 mm, in the X-Y plane, perpendicular to the axis of the torch.

Particle Surface Temperature. The in-flight surface temperature of the particles was determined by two-color pyrometry. Details of the experimental technique are given by Mishin (1985) and Mishin et al. (1987).

The experimental setup used is shown in Figure 2. Measurements were made of the particle emission at two wavelengths, 680.0 and 837.0 nm, using a pair of photomultipliers (Hamamatsu R928) of similar transient response characteristics. A monochromator (JYH10IR) placed in front of each of the photomultipliers was used to define the wavelength of the observed particle emission, and to block the background plasma radiation. In order to overcome the problems of coincidence requiring that the two photomultipliers be independently focused on the same particle in space, a beam splitter was used to project simultaneously the image of the particles on the entrance slit of each of the two monochromators.

Based on geometrical considerations, the measurement volume was estimated to be in the form of a parallelepiped of dimensions 1.5 × 20.0 mm in the X and Y directions, respectively, and 0.12 mm in the Z direction. The particularly long dimension in the Y direction is due to the fact that it represented

Table 1. Plasma Torch Operating Conditions

No.	Gas Flow Rate L/min	Current A	Voltage V	Power kW	Efficiency %	Sp. Enthalpy MJ/kg
1	75 (Ar)	490	35	17.1	53.0	4.46
2	75 (Ar) + 15 (H_2)	200	75	15.0	61.0	4.46
3	75 (Ar) + 15 (H_2)	400	73	29.2	60.0	8.50
4	45 (Ar) + 15 (H_2)	430	65	28.0	56.0	12.60

the line of sight of the optical setup used, which had a rather long depth of field. Reduction of the depth of field below this value would have required a larger objective lens that the 20 mm dia. lens presently used.

The passage of a particle in the measuring volume gives rise to two simultaneous electric pulses generated by each of the two photomultipliers. These are filtered and amplified using an Ortec 113 preamplifier and an Ortec 450 linear amplifier. An Ortec 464 analyzer is used to generate a signal that is proportional to the ratio of the amplitudes of the two pulses. Saturated signals, which generally reflect the presence of more than one particle in the measurement volume, are eliminated using a discriminator prior to statistical analysis of the signal using a multichannel analyzer (Northrop 5300).

By proper calibration of the apparatus using a standard tungsten ribbon lamp, the statistical information on the ratio of the particle emission at the two wavelengths can be converted into statistical informaton about the particle surface temperature distribution. While the measurements were reproducible within ±4%, the absolute precision of the temperatures obtained is estimated to be of the order of ±300 K at a particle surface temperature of 3,000 K. This is mainly due to a number of limiting factors, including uncertainties about the emissivity of the surface of the particles.

It should be emphasized that this technique, based on two-color pyrometry, for the determination of the in-flight particle surface temperature represents a major improvement over the technique previously used by Vardelle et al. (1983). It has, however, three principal limitations. The first is due to the background plasma radiation, which could not be tolerated beyond a certain critical value. No measurements could therefore be made in the bright core of the plasma jet at distances closer than 50 mm from the anode nozzle. The second limitation of the technique results from the rapid drop in the intensity of emission from the particle with the decrease of its surface temperature. The lower limit of the particle surface temperature that could be measured in the tail flame of the plasma jet was approximately 1,800 K. The third limitation was due to the relatively long depth of field in the direction of observation. Measurements therefore had to be limited to low powder feed rates, in order to reduce the possibility of having more than one particle at a time in the measuring volume, and consequently saturating the photoelectric system.

Results and Discussion

Measurements were carried out using Ar and Ar/H_2 plasmas under the conditions listed in Table 1. The powder was injected into the flow using a 2 mm ID powder feed port as indicated in Figure 1. The orientation of the injection port was in the positive X direction. Two types of alumina powders were used. These had the particle size distributions given in Figure 3. The mean particle diameter and the standard deviation for powders are respectively 18.0 ±3 μm and 60 ±15 μm.

The powder feed rate was approximately 4 g/min. Argon was used as a powder carrier gas with a flow rate that was varied between 4.5 and 8.5 L/min. Figure 4 shows the statistical distributions of the particle injection velocities, V_i, for each of the two alumina powders with different carrier gas flow rates. These were separately measured by laser Doppler anemometry in the absence of the plasma jet using a similar feed probe as that incorporated into the torch nozzle, Figure 1.

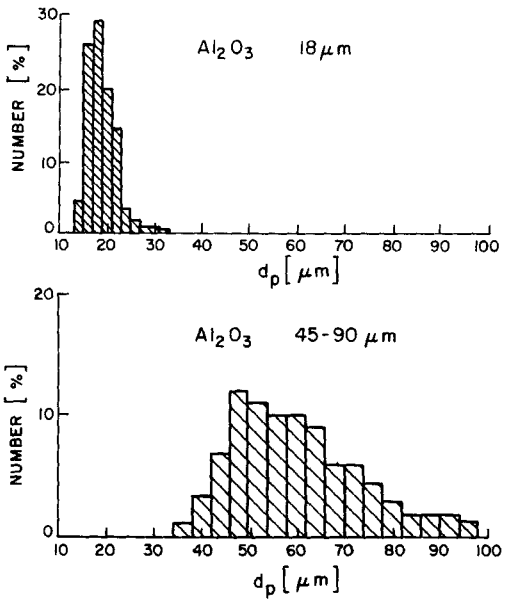

Figure 3. Particle size distributions of alumina powders used.
Top: Powder A, d_p = 18.0 ±3 μm
Bottom: Powder B, d_p = 60.0 ±15 μm

Particle trajectories

Typical particle trajectory data and particle flux number density distributions are given in Figure 5. These were obtained with the 18 μm dia. alumina powder injected into the plasma with a carrier gas flow rate of 5.5 L/min. The plasma operating conditions were those represented by case 3 of Table 1. Since a noncooled powder feed probe was used in this case, its tip was maintained at a distance of 4 mm from the edge of the nozzle (i.e., 8 mm from the axis of the jet) to avoid being damaged by the plasma heat.

It may be noted that in spite of the fact that the powder used

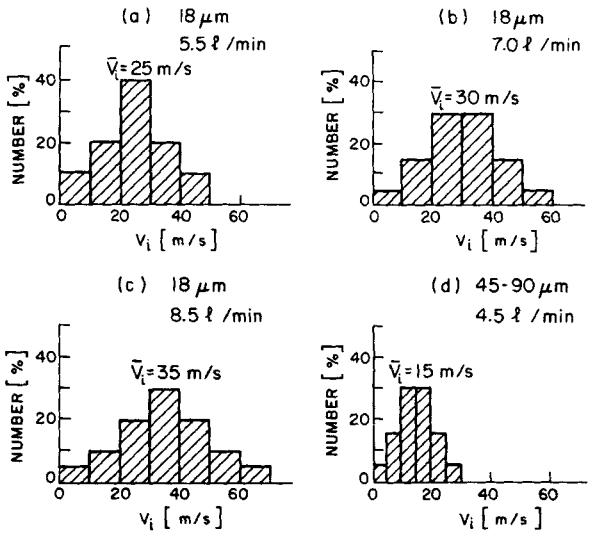

Figure 4. Statistical distributions of particle injection velocity V_i for two alumina powders at various carrier gas flow rates.

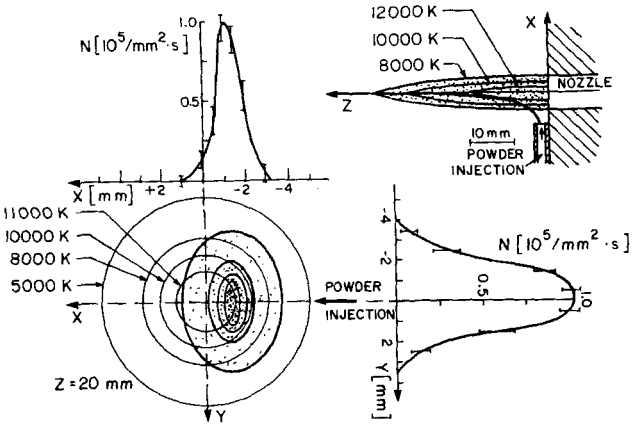

Figure 5. Particle trajectories and number flux distributions: noncooled injection probe 4 mm from edge of plasma jet.

Alumina powder, d_p = 18.0 ±3 μm; carrier gas flow rate, 5.5 L/min.

had a rather narrow particle size distribution (±3 μm), it spread over a large region of the plasma, as indicated by the particle flux isocontours given in the lower lefthand side of Figure 5. The corresponding profiles of the particle flux number densities in two orthogonal planes are given in the same figure. These show particle fluxes as high as 10^5 particles $(mm^2 \cdot s)^{-1}$ at the center of the particle stream, dropping off rather rapidly at the edge of the jet. It also shows an important asymmetry in the plane of injection (X direction) but with a relatively good symmetry in the orthogonal plane (Y direction).

It is interesting to compare the results given in Figure 5, obtained with a powder injection probe located 4 mm from the edge of the plasma jet, with those of Figure 6 in which, by using a water-cooled probe, it was possible to locate the point of injection of the powder right at the edge of the plasma jet. It is noticed that advancing the point of injection of the powder, even by only 4 mm, results in a substantial modification of the particle trajectories. For the same carrier gas flow rate (5.5 L/min), when injected at the edge of the jet the particles penetrate deeper into the plasma jet and have a better chance of heating and melting than when injected farther away.

The data given in Figure 6, also show that by increasing the powder carrier gas flow rate from 5.5 to 10.0 L/min, the alumina particles completely cross the axis of the plasma jet at a distance of approximately 8 mm from the point of injection.

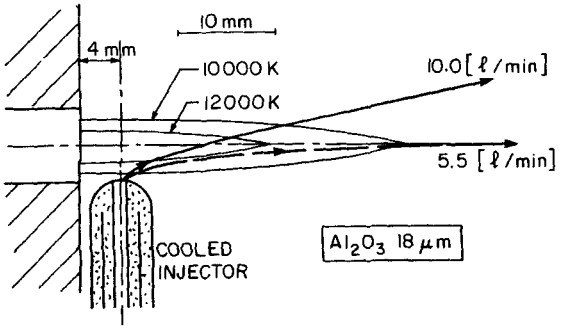

Figure 6. Particle trajectories: water-cooled powder injection probe at edge of jet.

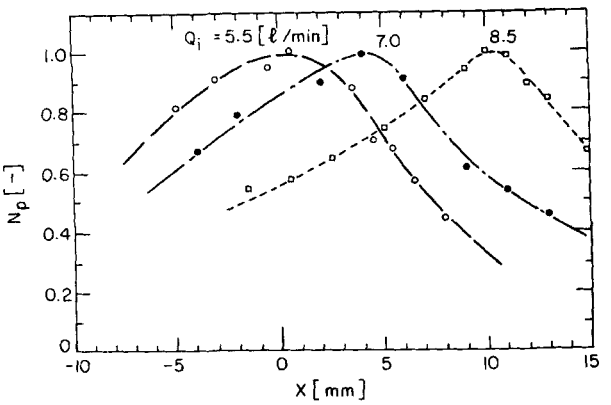

Figure 7. Particle number flux distributions at Z = 75 mm for various carrier gas flow rates.

Alumina, d_p ~ 18.0 ±3 μm; Ar/H_2 plasma, 29.2 kW.

It should be pointed out that the use of water-cooled powder injection probes can, however, have an important local cooling effect on the temperature field of the plasma flow around the point of injection. Such injection probes could also be responsible for the development of serious asymmetry of the flow and temperature fields in the plasma, as shown by Gravelle et al. (1987).

Particle flux number density, velocity, and surface temperature distributions

In order to determine the effect of variations of the plasma operating conditions and of the particle injection parameters on the particle flux number density, velocity, and surface temperature distributions, repeated measurements were carried out of the corresponding profiles in the X direction, at a fixed distance of 75 mm downstream of the nozzle.

Effect of Carrier Gas Flow Rate. Figures 7, 8, and 9 give respectively the particle flux number density, velocity, and surface temperature distributions for 18 μm dia. alumina powder, injected into the plasma with different carrier gas flow rates (5.5, 7.0, and 8.5 L/min). The plasma operating conditions were those of case 3 in Table 1 (i.e., Ar/H_2 plasma, 29.2 kW).

It may be noted that the highest particle velocities and temperatures were obtained at a relatively low carrier gas flow rate

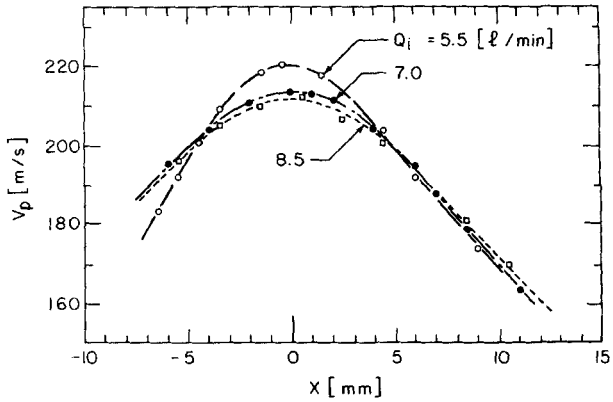

Figure 8. Particle velocity profiles at Z= 75 mm for various carrier gas flow rates.

Alumina, d_p= 18.0 ±3 μm; Ar/H_2 plasma, 29.2 kW.

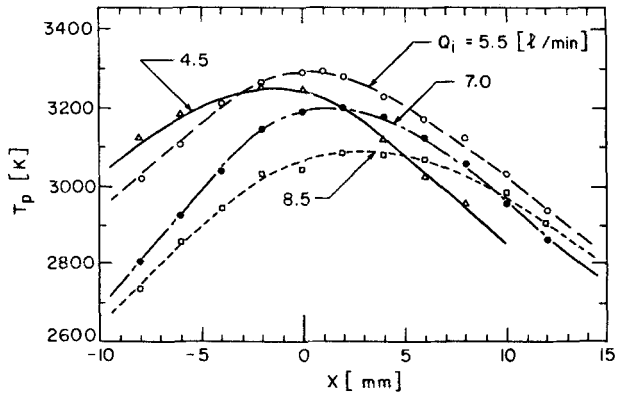

Figure 9. Particle surface temperature profiles at Z = 75 mm for various carrier gas flow rates.
Alumina, d_p = 18.0 ±3 μm; Ar/H_2 plasma, 29.2 kW.

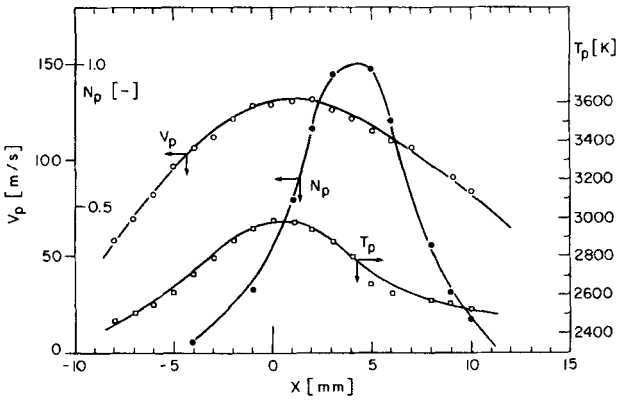

Figure 11. Particle number flux, velocity, and surface temperature profiles at Z = 75 mm.
Alumina, d_p = 18.0 ±3 μm; Ar plasma, 17.1 kW; Q_i = 5.5 L/min.

of 5.5 L/min. The corresponding particle flux density, given in Figure 7, shows that the particles in this case have an axial trajectory, with the maximum particle flux obtained on the centerline of the jet. Knowing that the plasma velocity and temperature are maximum in this region, it is reasonable to expect that the particles which acquire an axial trajectory along the centerline of the plasma jet would also acquire the highest velocity and surface temperature, compared to those moving along other trajectories.

It is interesting to note that, for the same reason, while increasing the carrier gas flow rate results in a substantial shift of the point of maximum particle flux, Figure 7, the maxima of the particle velocity and surface temperature profiles are always around the axis of the jet, Figures 8 and 9. It is the maximum values of the velocity and surface temperature attained by the particles that are affected by variations of the carrier gas flow rate, rather than their respective positions.

Similar results were also obtained with the larger diameter alumina powder, $45 < d_p < 90$ μm, under the same plasma operating conditions. The optimum carrier gas flow rate in this case was 4.5 L/min. The corresponding particle flux number density, velocity, and surface temperature profiles are given in Figure 10. Comparing these results with those obtained using the finer alumina powder, d_p = 18.0 ±3 μm, with their relatively narrow particle size distribution, it is noticed that both powders give rise to essentially similar distribution patterns in the flow. This can be attributed to the fact that particle trajectories in the jet are the result of a stochastic process involving the combined statistical distributions of the particle diameters and their injection velocities given in Figures 3 and 4, respectively.

Effect of the Nature of the Plasma Gas. In an attempt to determine the effect of the nature of the plasma gas, under comparable plasma specific enthalpy conditions, on the particle flux number density, velocity, and surface temperature distributions, measurements were carried out under plasma conditions 1 and 2 of Table 1. The results given in Figure 11 were obtained for a pure argon plasma with a specific enthalpy of 4.4 MJ/kg. The fine alumina powder was used in this case, d_p = 18.0 ±3 μm, and the powder carrier gas flow rate was set at 5.5 L/min. Figure 12 shows the corresponding results obtained using an Ar/H_2 plasma (17 vol. % H_2) with the same specific enthalpy, alumina powder, and powder injection conditions.

It may be noted that the maximum particle velocity obtained with an Ar/H_2 plasma is about 20–30% higher than that for a pure argon plasma with the same specific enthalpy. A similar effect is also observed for the maximum particle surface temperature, which reaches 2,970 K in a pure argon plasma, compared to 3,300 K for an Ar/H_2 plasma. This is mostly due to the sub-

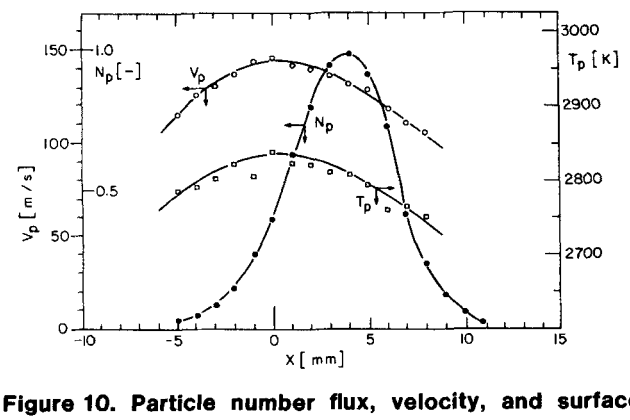

Figure 10. Particle number flux, velocity, and surface temperature profiles at Z = 75 mm.
Alumina, $45 < d_p < 90$ μm; Ar/H_2 plasma, 29.2 kW; Q_i = 4.5 L/min.

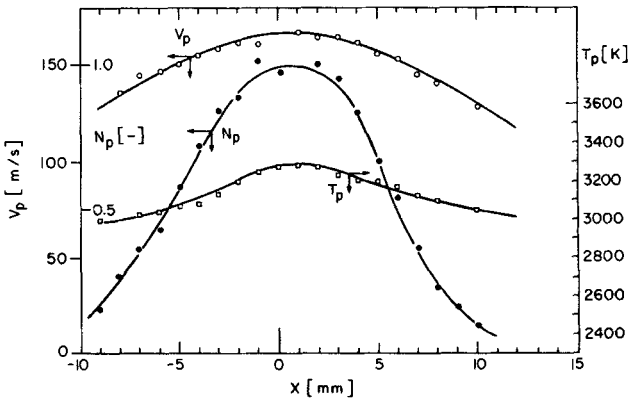

Figure 12. Particle number flux, velocity, and surface temperature profiles at Z = 75 mm.
Alumina, d_p = 18.0 ±3 μm; Ar/H_2 plasma, 15.0 kW; Q_i = 5.5 L/min.

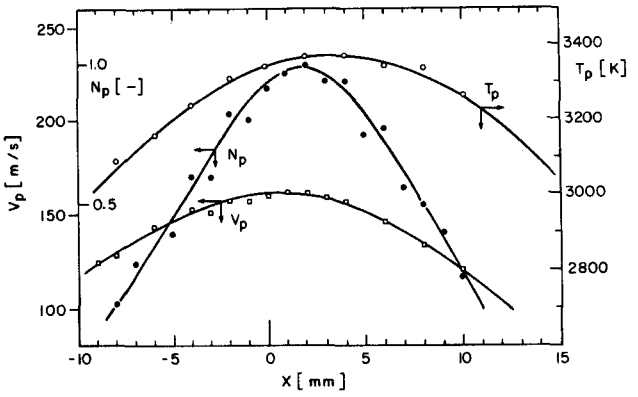

Figure 13. Particle number flux, velocity, and surface temperature profiles at Z = 75 mm.
Alumina, d_p = 18.0 ±3 μm; Q_i = 5.5 L/min
Ar/H_2 plasma, plasma gas flow rate = 60 L/min, 28.0 kW.

stantial increase of the plasma-particle heat transfer coefficients as a result of the addition of small percentages of hydrogen into the plasma gas, as discussed by Bourdin et al. (1983).

It is also to be noticed that the particle distribution is wider and better centered in relation to the axis of the jet with the Ar/H_2 plasma, compared to that for a pure argon plasma. This may also be due to the high plasma-particle momentum transfer in an Ar/H_2 plasma.

Effect of Plasma Gas Flow Rate. Figures 13 and 14 give the results of measurements of the particle number flux, velocity, and surface temperature distributions for the fine alumina powder, d_p = 18.0 ±3 μm, with Q_i = 5.5 L/min, for an Ar/H_2 plasma at total plasma gas flow rates of 60 and 90 L/min (conditions 3 and 4, Table 1).

As expected, the increase of the plasma gas flow rate results in a substantial increase of the particle velocity by almost 40%. The particle surface temperature, however, shows only a slight drop of approximately 100 K with the increase of the plasma gas flow rate. While the effect is relatively small, it could be attributed to the lower specific enthalpy of the plasma and the shorter residence time of the particles in the higher flow rate plasma jet, compared to that at the lower plasma gas flow rate.

It is interesting to note that the advantages associated with

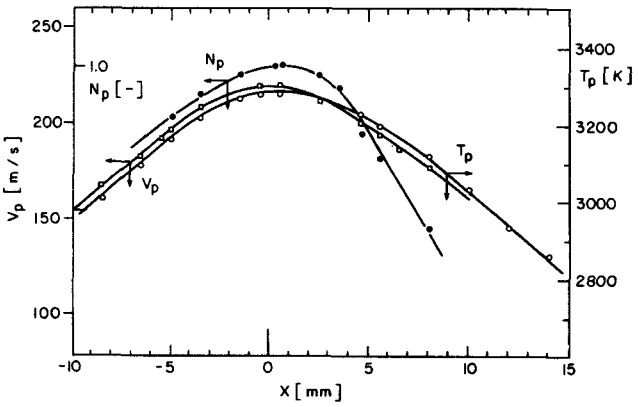

Figure 14. Particle number flux, velocity, and surface temperature profiles at Z = 75 mm.
Alumina, d_p = 18.0 ±3 μm; Q_i = 5.5 L/min
Ar/H_2 plasma, plasma gas flow rate = 90 L/min, 29.2 kW

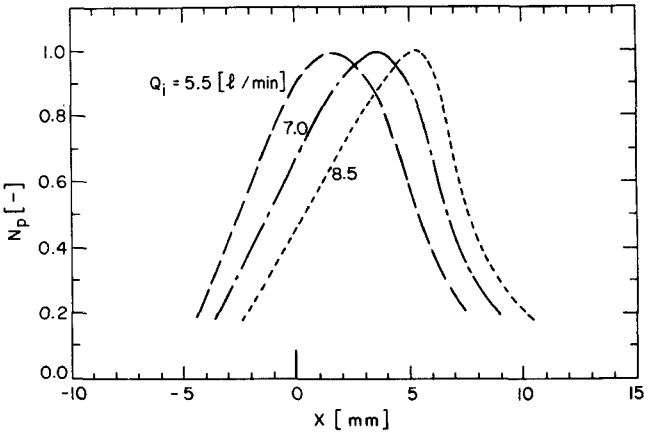

Figure 15. Particle number flux distributions at Z = 75 mm for various carrier gas flow rates.
Alumina, d_p = 18.0 ±3 μm; Ar/H_2 plasma, 29.2 kW

the higher plasma gas flow rate, as indicated by the higher particle velocity, and the more uniform distribution of the particle flux number density in the plasma jet, are reflected in the improved quality of the alumina deposits obtained in a plasma spray-coating operation using these conditions.

Mathematical Modeling

Computations were carried out of single particle trajectories and temperature history based on the following assumptions:

- The injected powder is composed of spherical particles of known particle size distribution
- Particle trajectories are governed by the inertia and drag forces
- Dilute system, with negligible plasma-particle and particle-particle interactions

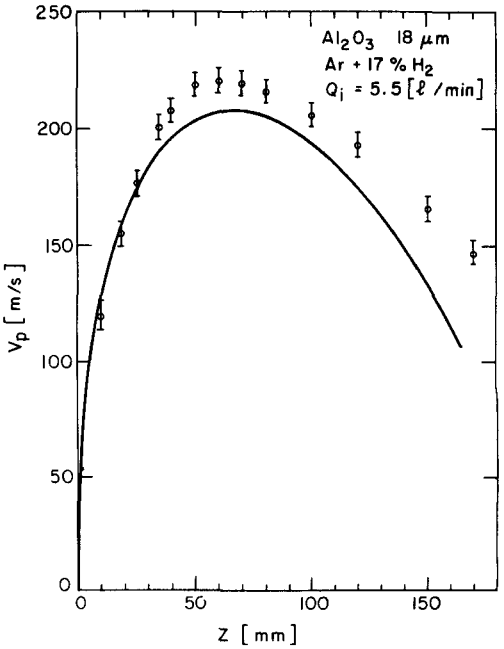

Figure 16. Experimental and computed axial particle velocity profiles along centerline of plasma jet.
P = 29.2 kW

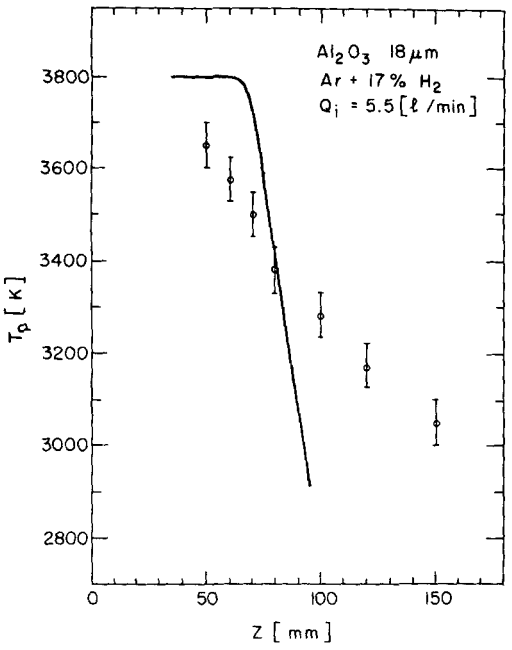

Figure 17. Experimental and computed axial particle temperature profiles along centerline of plasma jet.
P = 29.2 kW

• Known plasma velocity and temperature fields (experimentally determined: Vardelle et al., 1983; Vardelle et al., 1980)

The effect of the presence of steep temperature gradients on the plasma-particle momentum and heat transfer was accounted for using an integral average of the plasma transport properties across the boundary layer surrounding the particle (Bourdin et al., 1983). Whenever applicable, modification of the drag and heat transfer coefficients due to evaporation and the Knudsen effects (Chen and Pfender, 1982a,b, 1983a,b) was included. The governing equations and details of the computation scheme are described elsewhere (Boulos and Fauchais, 1986; Vardelle et al., 1986).

Typical results, in terms of the particle flux number density distributions at Z = 75 mm, for fine alumina powder (d_p = 18.0 ±3 μm) at different carrier gas flow rates, are given in Figure 15. The plasma gas in the case was Ar/H_2 with a total flow rate of 90.0 L/min. The plasma power was 29.2 kW (condition 3, Table 1).

From a comparison of these results with the experimental data given in Figure 7 for the same plasma and particle operating conditions, the following observations may be noted. Globally, the model predictions show the same trends as the experimental data. The computed particle flux distributions, however, are considerably narrower than the measured distributions. This could be attributed mainly to the fact that the present model did not include turbulent diffusion effects, which—for the relatively small size of the particles studied—could be important.

A comparison between the computed and the experimental particle velocity and temperature profiles along the centerline of the plasma jet is given in Figures 16 and 17, respectively. These show a reasonably good agreement as far as the particle velocity is concerned. The computed particle surface temperature, however, while being close to the experimental values in the early part of the trajectory, show a considerably faster particle cooling rate than that experimentally observed. The difference could be related to uncertainties in the prediction of radiative heat losses from the particles, which can be important in this temperature range. The agreement between the model predictions and the experimental data is, however, considerably better than the results reported by Vardelle et al. (1983). Further refinement of both the experimental technique and the development of the theoretical model is still needed. Special attention is to be given to a better estimation of the effects of internal heat conduction into the particle, especially for porous particles, and of radiation heat losses from the surface of the particle.

Acknowledgment

This work was partially supported by the French and Quebec governments through a France-Quebec Scientific Exchange Program, and by E.D.F. (Electricité de France).

Notation

d_p = particle diameter, μm
N = particle number flux density, particle/mm² · s
N_p = normalized particle number flux
Q_i = powder carrier gas flow rate, L/min
T_p = particle surface temperature, K
V_i = particle injection velocity, m/s
V_p = particle velocity in axial direction, m/s
X = distance in X direction, mm
Y = distance in Y direction, mm
Z = distance in Z direction, mm

Literature Cited

Boulos, M. I., and P. Fauchais, "Transport Processes in Thermal Plasmas," *Advances in Transport Processes*, Wiley Eastern Ltd., **4**, 274 (1986).

Boulos, M. I., P. Fauchais, and E. Pfender, "Diagnostic Techniques in Thermal Plasma Processing," DOE Rpt. ER-0270 (Feb., 1986).

Bourdin, E., P. Fauchais and M. I. Boulos, "Transient Heat Conduction to a Single Sphere Under Plasma Conditions," *Int. J. Heat Mass Trans.*, **26**, 567 (1983).

Chen, X., and E. Pfender, "Heat Transfer to a Single-Particle Exposed to a Thermal Plasma," *Plasma Chem. Plasma Proc.*, **2**, 185 (1982a).

———, "Unsteady Heating and Radiation Effects of Small Particles in a Thermal Plasma," *Plasma Chem. Plasma Proc.*, **2**, 293 (1982b).

———, "Behavior of Small particles in a Thermal Plasma Flow," *Plasma Chem. Plasma Proc.*, **3**, 351 (1983a).

———, "Effect of the Knudsen Number on Heat Transfer to a Particle Immersed into a Thermal Plasma," *Plasma Chem. Plasma Proc.*, **3**, 97 (1983b).

Gravelle, D., M. Beaulieu, C. Carlone, and M. I. Boulos, "Three-Dimensional Temperature Measurements in an Asymmetric d.c. Plasma Jet", to be published (1987).

Mishin, J., "Contribution à la Mise au Point d'un Dispositif de Mesure des Températures de Surface des Particules en Vol dans un Jet de Plasma d'Arc," Thèse de Doctorat, 3ième cycle, Univ. Limoges, France (1985).

Mishin, J., M. Vardelle, J. Lesinski, and P. Fauchais, "Two-color Pyrometer for the Statistical Measurement of Particulate Surface Temperature Under Thermal Plasma Conditions," *J. Phys. E., Sci. Instruments*, **20** (1987).

Vardelle, A., J. M. Baronnet, M. Vardelle, and P. Fauchais, "Measurements of the Plasma and Condensed Particles Parameters in a d.c. Plasma Jet," *IEEE Trans. Plasma Sci.*, **8**, 417 (1980).

Vardelle, M., A. Vardelle, P. Fauchais, and M. I. Boulos, "Plasma-Particle Momentum and Heat Transfer: Modeling and Measurements," *AIChE J*, **29**, 236 (1983).

Vardelle, A., M. Vardelle, and P. Fauchais, "Les Transferts de Quantité de Mouvement et de Chaleur Plasma Particules dans un Plasma d'Arc en Extinction," *Revue Int. Hautes Temp. et Réfractaires*, **23**, 69 (1986).

Manuscript received May 15, 1987, and revision received Oct. 12, 1987.